



## The pentapeptide LQVVR plays a pivotal role in human cystatin C fibrillization



Paraskevi L. Tsiolaki, Stavros J. Hamodrakas, Vassiliki A. Iconomidou \*

Department of Cell Biology and Biophysics, Faculty of Biology, University of Athens, Panepistimiopolis, Athens 157 01, Greece

### ARTICLE INFO

#### Article history:

Received 1 October 2014  
Revised 10 November 2014  
Accepted 19 November 2014  
Available online 3 December 2014

Edited by Jesus Avila

#### Keywords:

Human cystatin C  
Hereditary Cystatin C Amyloid Angiopathy  
Alzheimer's disease  
3D-domain swapping  
'Aggregation-prone' pentapeptide LQVVR  
Amyloid fibrils

### ABSTRACT

**Human cystatin C (HCC) is a low molecular weight member of the cystatin family (type2). HCC consists of 120 amino acids. Normally it is an inhibitor of cysteine proteases, but in pathological conditions it forms amyloid fibrils in brain arteries of young adults. An 'aggregation-prone' pentapeptide (<sup>47</sup>LQVVR<sup>51</sup>) was located within the HCC sequence using AmylPred, an 'aggregation-prone' peptide prediction algorithm developed in our lab. This peptide was synthesized and self-assembled into amyloid-like fibrils in vitro, as electron microscopy, X-ray fiber diffraction, Attenuated Total Reflectance Fourier-Transform Spectroscopy and Congo red staining studies reveal. Thus, the <sup>47</sup>LQVVR<sup>51</sup> peptide seems to have an important role in HCC fibrillization.**

© 2014 Published by Elsevier B.V. on behalf of the Federation of European Biochemical Societies.

### 1. Introduction

Human cystatins are proteins that have the capacity to regulate normal body processes and usually their down-regulation causes several diseases [1]. The first cystatin sequence determined was that for a protein isolated from human urine, which was first called  $\gamma$ -trace due to its electrophoretic mobility and it was later renamed cystatin C [2]. Cystatins form a single chain 'superfamily' of reversible inhibitors of cysteine proteases of the papain-like (C1) and legumain-related (C13) families, which consists of three major types, with proteins homologous in sequence [3]. These groups, based on molecular organization, have different distributions in an organism. It is obvious that evolutionary pressure has created different branches of cystatins by duplication events far back in time. Today, we know that cystatins are present in many kinds of eukaryotic organisms such as mammals, birds, fish, insects, plants and some protozoa [4]. The basic structural fold of monomeric representatives of the cystatin superfamily has been defined by the crystal structure of chicken cystatin [5].

Human cystatin C (HCC) is a low molecular weight protein which belongs to the cystatin family [6]. HCC, expressed in all nucleated human cells, is a secretory type 2 cystatin, and it has, predominantly, extracellular functions. It is widely used as an endogenous marker of several illnesses since its presence in all types of cells seems to be independent of age, sex and muscle mass. It is found in all tissues and body fluids [4] and it is present at particularly high concentrations in cerebrospinal fluid [2,6]. It consists of a polypeptide chain of 120 amino acid residues [3] and its canonical structural features include a long alpha helix ( $\alpha$ 1 helix) running across a large, five-stranded antiparallel beta-sheet (Fig. 1). Recently, a monomer-stabilized HCC with an engineered disulfide bond [(L47C)–(G69C)] has been created by Koladziejczyk et al. [5]. Three regions are implicated in its interaction with the enzyme papain family: The N-terminal segment and the two hairpin loops L1 and L2, constitute a structural epitope, which shows high affinity and binds to the enzyme [7] (Fig. 1).

HCC is co-deposited in the amyloid plaques of Alzheimer's disease and Down's syndrome [8] and it is also involved in tissue-degenerative diseases such as osteoporosis and periodontitis [9]. In pathological processes, it forms amyloid deposits in brain arteries of young adults, which lead to fatal cerebral hemorrhage. In advanced age, under denaturing conditions the protein oligomerization leads to amyloid deposits in the leptomeninges, cerebral cortex and brainstem [10]. These amyloid fibrils are composed of a mutated and truncated variant of cystatin C that eventually

Abbreviations: HCC, human cystatin C; HCCAA, Hereditary Cystatin C Amyloid Angiopathy; ATR FT-IR Spectroscopy, Attenuated Total Reflectance Fourier-Transform Spectroscopy

\* Corresponding author. Fax: +30 210 7274254.

E-mail address: [veconom@biol.uoa.gr](mailto:veconom@biol.uoa.gr) (V.A. Iconomidou).

accumulates to cause hemorrhage and death. The corresponding amyloidosis is called Hereditary Cystatin C Cerebral Amyloid Angiopathy (Icelandic Cerebral Angiopathy) and it seems to be the first familial type of amyloidosis related to a point mutation in a gene coding for an inhibitor [11–13]. This angiopathy is an autosomal dominant disorder found in members of 8 different families originating from one specific geographical area in Iceland [14,15].

Three crucial events turn the wild type protein into a pathological form. First, a point mutation (A → T) at codon 68 of cystatin C gene (located on chromosome 20) converts a leucine to glutamine (L68Q), leading to an amino acid substitution. Leucine 68 is located at the C-terminal end of strand  $\beta$ 3 and its side-chain participates in the hydrophobic core that stabilizes the protein, between the  $\alpha$ -helix and the five-stranded  $\beta$ -sheet [16] (Fig. 1). In the case of the mutant L68Q, the amino acid substitution affects greatly the stability of the molecule, because the long polar side chain of glutamine cannot be accommodated into the hydrophobic core of HCC (Figs. 1 and S1). Secondly, human amyloid deposits have an N-terminal truncation possibly because of the disintegration of the leucocytes, normally present in the cerebrospinal fluid. Proteolytic enzymes take action and remove the first 10 amino acids residues of the native sequence of HCC [14,17]. Finally, replacement of the hydrophobic Leu68 promotes unfolding through the L1 loop with a specific mechanism named 3D-domain swapping [18] (Supplementary Fig. S1). From the time of its definition it has been observed in different proteins; among them in the amyloidogenic proteins prion and  $\beta$ 2-microglobulin [19,20].

In the case of cystatin C, the L1 loop is the segment of the protein, which connects the swapped domain to the rest of the protein and actually the one segment which changes its conformation between the monomer and the oligomer. Two identical monomers exchange equivalent structural components and form a closed interface, which is identical in the monomer and dimer, with the exception that in the oligomer two separate polypeptide chains contribute to the interaction [19] (Supplementary Fig. S1). This mechanism for protein homo-oligomerization may be involved in the fibrillogenesis in the case of angiopathy [17].

Amyloids are formed under protein-denaturing conditions or as a result of mutations, as in HCC. The conversion of amyloidogenic proteins from their soluble forms into fibrillar aggregates is associated with a wide range of pathological conditions [21–24]. As research continues for the understanding of the mechanisms involved in amyloid formation, the development of prediction methods is an important complement to experimental approaches [23]. Detailed theoretical and experimental evidence has repeatedly indicated that amyloid formation is mediated by specific short sequence regions/stretches of a polypeptide chain that have a higher aggregation propensity and therefore vitally contribute to its aggregation tendency [25–27]. In this work, we determined a novel aggregation-potent segment of HCC,  $^{47}\text{LQVVR}^{51}$ , which was initially predicted as such, by implementing AMYLPRED, our aggregation propensity prediction algorithm [28]. This ‘aggregation-prone’ peptide segment was synthesized (see Section 2) and here we present experimental results, verifying its strong aggregation propensity to form amyloid fibrils. Also, we discuss our findings, implicating LQVVR as one of the main driving forces in HCC fibril formation, providing a novel target for HCC amyloidosis prevention/prohibition.

## 2. Materials and methods

### 2.1. Peptide synthesis and formation of amyloid-like fibrils

The LQVVR peptide-analogue, part of the 2nd beta-strand of cystatin C (Fig. 1) was synthesized by GeneCust Europe, Luxembourg

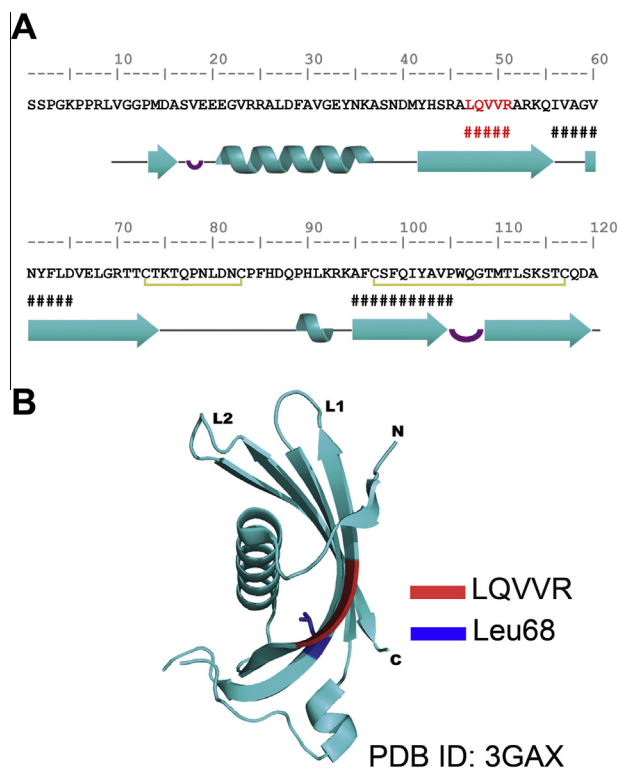


**Fig. 1.** Amino acid sequence and native structure of human cystatin C. (A) The polypeptide sequence normally consists of 120 amino acid residues [3]. In the case of Cerebral Amyloid Angiopathy, proteolytic enzymes, which are present in the cerebrospinal fluid, remove the first 10 amino acids, at the N-terminal of the native sequence [14,17]. Predicted ‘aggregation-prone’ segments by AMYLPRED [28], are shown in red ( $^{47}\text{LQVVR}^{51}$ ) and bold ( $^{56}\text{IVAGVNYFLD}^{65}$  and  $^{95}\text{AFCSQIYAVP}^{105}$ ), respectively, and are marked with “#” under the sequence. Dark yellow lines point out existing disulfide bonds. (B) A monomer-stabilized human cystatin C with an engineered disulfide bond (see Section 1) is shown (PDB ID: 3GAX) [5], based on the crystal structure of chicken cystatin [7]. L1 and L2 hairpin loops and the N-terminal segment, indicate the structural epitope of the protein, capable of binding to cysteine proteases. Colored regions in red and dark blue, illustrate the  $^{47}\text{LQVVR}^{51}$  ‘aggregation-prone’ segment and Leucine 68, respectively.

(98% pure, free N- and C-terminals). The synthesized LQVVR peptide was dissolved in distilled water (pH 5.5), at a concentration of 10 mg/ml to produce mature amyloid-like fibrils after 1–2 weeks incubation. Oriented fibers, suitable for X-ray diffraction, were obtained from suspensions of LQVVR mature amyloid-like fibrils, as described below.

### 2.2. X-ray diffraction

A droplet (~10  $\mu$ l) of mature fibril suspension was placed between two siliconized glass rods, spaced ~1.5 mm apart and mounted horizontally on a glass substrate, as collinearly as possible. The droplet was allowed to dry slowly at ambient temperature and humidity for 1 h to form an oriented fiber, suitable for X-ray diffraction. X-ray diffraction patterns were recorded on a Mar Research 345 mm image plate, utilizing  $\text{CuK}\alpha$  radiation ( $\lambda = 1.5418 \text{ \AA}$ ), obtained from a Rigaku MicroMax-007 HF, microfocus rotating anode generator (with Osmic Rigaku VariMax<sup>TM</sup> HF optics), operated at 40 kV, 20 mA. The specimen-to-film distance was set at 150 mm and the exposure time was 30 min. No additional low angle reflections were observed at longer specimen-to-film distances, up to 300 mm. The X-ray patterns, initially viewed using the program MarView (MAR Research, Hamburg, Germany), were displayed and measured with the aid of the program IPDISP of the CCP4 package [29].

### 2.3. Negative staining

For negative staining, LQVVR peptide mature fibril suspensions were applied to glow-discharged 400-mesh carbon-coated copper grids for 60 s. The grids were (occasionally) flash-washed with  $\sim 150 \mu\text{l}$  of distilled water and stained with a drop of 1% (w/v) aqueous uranyl acetate for 45 s. Excess stain was removed by blotting with a filter paper and the grids were air-dried. They were examined in a Philips CM120 BioTWIN transmission electron microscope (FEI, Eindhoven, The Netherlands) operated at 100 kV. Photographs were obtained with a bottom-mounted Keen View 1K CCD camera (Soft Imaging System, Muenster, Germany).

### 2.4. Attenuated total reflectance Fourier-transform infrared spectroscopy (ATR FT-IR) and post-run computations of the spectra

A 10- $\mu\text{l}$  drop of the HCC-analogue, LQVVR, mature fibril suspension was cast on a front-coated Au mirror and left to dry slowly at ambient conditions to form a thin film. Infrared spectra were obtained from these films at a resolution of  $4 \text{ cm}^{-1}$ , utilizing an IR microscope (IRScope II by Bruker Optics) equipped with a Ge attenuated total reflectance (ATR) objective lens ( $20\times$ ) and attached to a Fourier-transform infrared (FTIR) spectrometer (Equinox 55, by Bruker Optics). Internal reflection spectroscopy has several advantages compared with the more common KBr dispersion technique [30]. The choice of ATR was dictated by the need to exclude any possible spectroscopic and chemical interactions between the sample and the dispersing medium. Having a penetration depth ca. 1–2  $\mu\text{m}$  ( $1000 \text{ cm}^{-1}$ , Ge), ATR is free of saturation effects, which may be present in the transmission spectra of thicker samples. Moreover, the use of a microscope facilitates the acquisition of data from small samples. Ten 32-scan spectra were collected from each sample and averaged to improve the S/N ratio. The spectra are shown in the absorption mode after correction for the wavelength dependence of the penetration depth ( $pd \sim \lambda$ ). Absorption band maxima were determined from the minima in the second derivative of the corresponding spectra. Derivatives were computed analytically using routines of the Bruker OPUS/OS2 software and included smoothing by the Savitzky–Golay algorithm [31] over a  $\pm 8 \text{ cm}^{-1}$  range, around each data point. Smoothing over narrower ranges resulted in a deterioration of the S/N ratio and did not increase the number of minima that could be determined with confidence.

### 2.5. Congo red staining and polarized light microscopy

HCC mature fibril suspensions were applied to glass slides and stained with a 10 mM Congo Red (Sigma) solution in PBS (phosphate-buffered saline, pH 7.4) for approximately 30 min. Then, they were washed several times with 90% ethanol and left to dry approximately for 10 min. The samples were observed under bright field illumination and between cross polars, using a Leica MZ75 polarizing stereomicroscope, equipped with a JVC GC-X3E camera.

### 2.6. Crystallization experiments and polarized light microscopy

Quantities of freshly made LQVVR peptide solutions in distilled water (concentrations 5–10 mg/ml, pH 5.5) were tested in crystallization experiments, using the “hanging-drop” method [32], for the possible formation of crystals. The precipitant was  $(\text{NH}_4)_2\text{SO}_4$  (concentration varied from 1.0 to 2.0 M). The samples were observed, both under bright field illumination and between crossed polars, respectively, using a Leica MZ75 polarizing stereomicroscope (please, see [Supplementary Data](#)).

### 2.7. Structural models

The HCC models were built from PDB files 3GAX, 1R4C and 1G96 [33]. The software PyMol [34] was used to visualize and manipulate the models.

## 3. Results

Electron micrographs of LQVVR peptide fibrils show protofilaments, which are straight, unbranched and coalesce laterally among each other to form ribbons (or tapes). The protofilaments have a diameter of approximately  $\sim 30 \text{ \AA}$  (Fig. 2). Congo red stained LQVVR peptide fibrils showed the red–green birefringence characteristic of amyloid fibrils, when viewed under crossed polars (Fig. 3). Additionally, X-ray diffraction patterns from fibers formed from LQVVR peptide fibrils showed two strong reflections at 4.62  $\text{\AA}$  and 11.63  $\text{\AA}$  (Fig. 4). These reflections appear as rings due to the poor alignment of the constituent fibrils. This is probably due to random packing of the fibers in the gels which adopt all possible orientations as confirmed by electron microscopy. The strong reflection at 4.62  $\text{\AA}$  suggests that  $\beta$ -sheets are present and it is attributed to inter-strand distances. The weaker reflection at 11.63  $\text{\AA}$  most probably corresponds to the inter-sheet packing distances. These two reflections clearly indicate the existence of  $\beta$ -sheets and are characteristic of the cross- $\beta$  conformation observed for several amyloid-like fibrils (Fig. 4), not oriented, however, in this case. The ATR FT-IR spectrum (Fig. 5) shows a prominent band at  $1634 \text{ cm}^{-1}$  in the amide I region, which is a band clearly due to  $\beta$ -sheet conformation and the shoulder at  $1697 \text{ cm}^{-1}$  is an indication that the  $\beta$ -sheets are antiparallel [35–39]. Thus, this spectrum supports the presence of antiparallel  $\beta$ -sheets in the structure of the LQVVR peptide fibrils, apparently in agreement with the existence of  $\beta$ -sheet structure suggested by X-ray diffraction and Congo red binding data (Table 1).

## 4. Discussion

Our experimental work clearly shows that fibrils formed from LQVVR peptide solutions fulfill all three basic criteria of amyloid fibrils: they are straight and unbranched, they bind the dye Congo Red exhibiting the characteristic for amyloids ‘red-apple/green’ birefringence, and oriented fibers made-up of them give characteristic ‘cross- $\beta$ ’ – like X-ray diffraction patterns [24].

Several fibrillogenesis pathways of peptides or proteins have been proposed during the last two decades and many concepts have been described for the in vitro or in vivo formation of amyloid

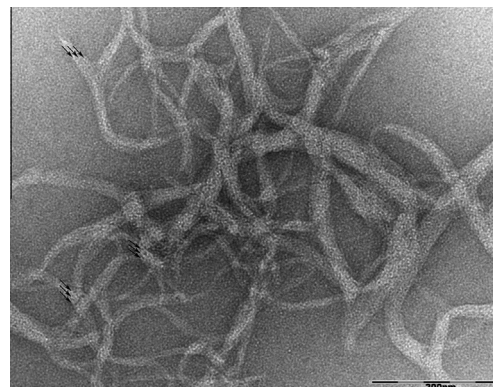


**Fig. 2.** Transmission electron microscopy images of negatively stained LQVVR amyloid-like fibrils, forming ribbons (see Section 3). Individual fibrils are indicated with multiple black arrows (ca. 30–40  $\text{\AA}$  in diameter). Bar is 200 nm.

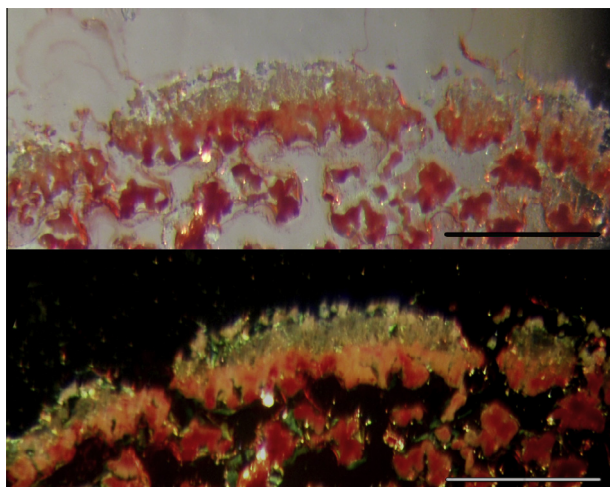


**Fig. 3.** A 10 mg/ml solution of the LQVVR peptide was incubated in distilled water (at ambient temperatures, pH 5.5), for approximately 10 days to produce mature amyloid-like fibrils and then it was stained with Congo Red. Mature amyloid-like fibrils appear red under bright field illumination and exhibit a strong green-apple birefringence under crossed polars. Bar is 500  $\mu\text{m}$ .

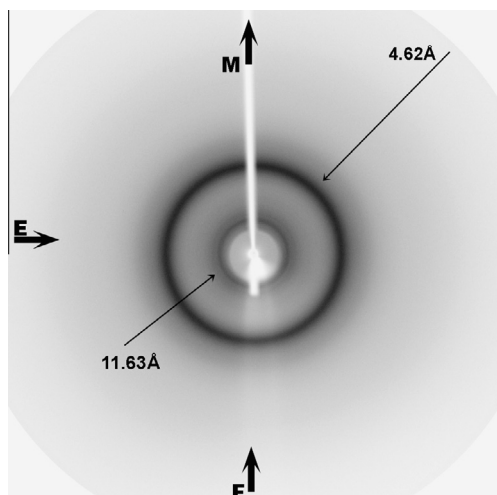


**Fig. 4.** X-ray diffraction pattern from aligned LQVVR peptide mature amyloid-like fibrils. Reflections with spacings of 4.62 Å and 11.63 Å, respectively, are indicated with arrows. Diffraction patterns were acquired using a Rigaku MicroMax-007 microfocus rotating anode generator (with Osmic Rigaku VariMax™ HF optics), operated at 40 kV, 20 mA.

protofilaments and fibrils [40–43]. Supramolecular spherical structures, known as spherulites were formed after 1 day incubation of LQVVR under a wide variety of conditions (Supplementary Fig. S2). As we have proposed in 2004 [44] the first main step of amyloid-like fibrillogenesis is the formation of a nuclei of liquid crystalline nature, in several cases. Spherulites were observed in a polarizing microscope under crossed polars with characteristic ‘maltese crosses’ [45,46]. In a similar fashion we might assume that these liquid crystalline intermediates of LQVVR were transformed into amyloid-like fibrils (Supplementary Fig. S2). Electron micrographs of mature fibrils, obtained from solutions of the LQVVR peptide, after 1–2 weeks incubation, show protofilaments associated laterally to form multistranded ribbons (or tapes). The protofilaments have a thickness of approximately 30 Å, almost at the resolution limit of the electron microscope (Fig. 2).

The propensity of the wild type (wt) HCC and of the mutated form L68Q to form fibrils in vitro were tested by Wahlbom et al.

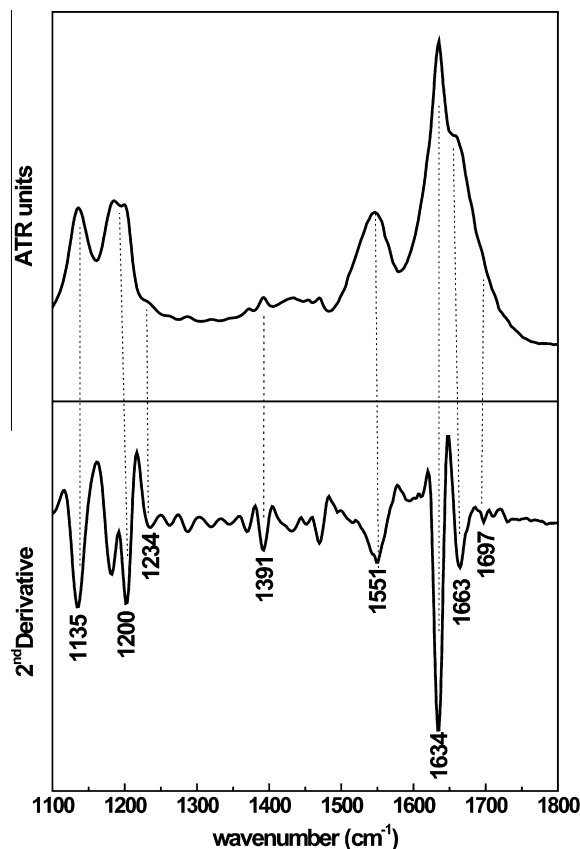


**Fig. 5.** ATR FT-IR (1100–1800  $\text{cm}^{-1}$ ) spectrum of LQVVR peptide mature amyloid fibrils, cast on a flat stainless-steel plate and left to air-dry slowly, at ambient conditions, to form a hydrated, thin film. A second derivative spectrum is also included.

**Table 1**

Bands observed in the ATR FT-IR (1500–1800  $\text{cm}^{-1}$ ) spectrum produced from a hydrated film of the ‘aggregation-prone’ pentapeptide, LQVVR, after self-assembly, and their tentative assignments (Fig. 5).

Band ( $\text{cm}^{-1}$ )	Assignment
1135	TFA
1200	TFA
1234	Amide III ( $\beta$ -sheet)
1391	
1551	Amide II ( $\beta$ -sheet)
1634	Amide I ( $\beta$ -sheet)
1663	TFA
1697	Amide I (antiparallel $\beta$ -sheet)

[47]. The wt protein forms long, twisted fibrils with a diameter of 100–120 Å, at pH 4, whereas the mutated protein forms fibrils with the same appearance to those of the wt protein, but with a higher tendency for lateral attachment.

Amyloid aggregation is actually driven by short fragments of misfolded proteins (“amyloid stretch hypothesis”) [25–27]. Short amyloidogenic stretches of five or six amino acid residues provide the potential to ‘guide’ amyloid fibril formation from a soluble globular domain. Therefore, several algorithms have been published during the last decade or so, which attempt to predict such ‘aggregation-prone’ stretches based on various properties of peptide chains. A relatively recent review of available software is given in Ref. [23]. Utilizing our consensus prediction algorithm of ‘aggregation-prone’ segments AMYLPRED [28], three (3) peptides of HCC were predicted as ‘aggregation-prone’ segments: The

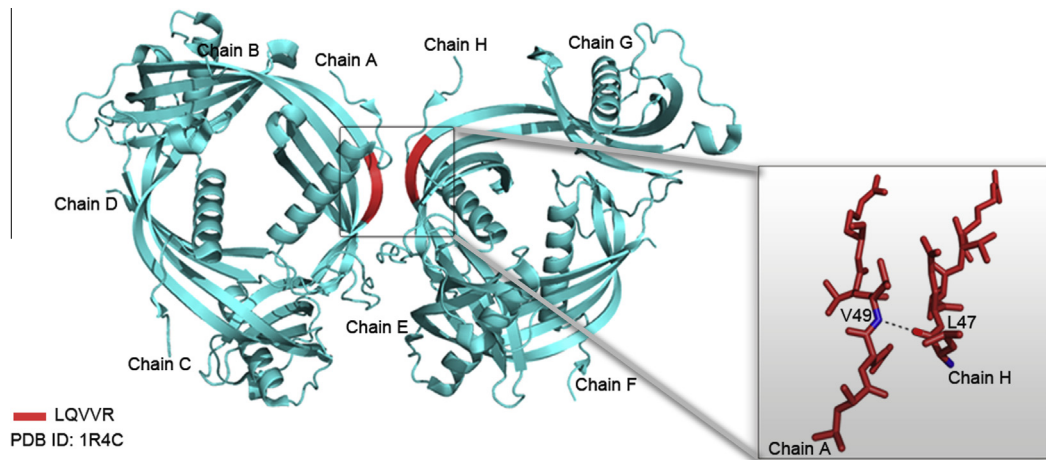


**Fig. 6.** Crystal structure of the domain swapped octamer of N-truncated HCC (PDB ID: 1R4C). Two tetramers interact together via two LQVVR pentapeptides (in red) to form an octamer. Red sticks represent the atomic structure of the LQVVR peptide, both backbone and side chains. A dashed line connects the main chain carbonyl O atom (bright red) of Leu 47 (chain H) and the main chain N atom (blue) of Val49 (chain A), indicating a possible hydrogen bond between the two donut shaped tetramers.

pentapeptide  $^{47}\text{LQVVR}^{51}$  and the peptides  $^{56}\text{IVAGVNYFPLD}^{65}$  and  $^{95}\text{AFCSFQIYAVP}^{105}$  (Fig. 1). All three peptides were synthesized and the LQVVR peptide was shown conclusively to have amyloidogenic properties (see Section 3), whereas for the other two peptides work is in progress to determine their amyloidogenic properties (*data in preparation*).

Amyloid deposits of patients in cerebrospinal fluid contain HCC, shortened by ten amino acid residues at the N-terminal segment because of disintegration of proteolytic leucocyte enzymes, which are normally present in this fluid [17]. Janowski et al. [17] managed to crystallize this N-truncated form of HCC and solve its crystal structure (PDB ID 1R4C). They discovered that this form of HCC forms domain swapped dimers of HCC (Supplementary Fig. S1), which in turn form tetramers and the tetramers in turn associate to form octamers (Fig. 6). It was very interesting to note that tetramers interact via the highly amyloidogenic LQVVR peptide to form octamers (Fig. 6). It is noteworthy that the ‘aggregation-prone’ peptide LQVVR lies exposed on the surface of the tetramers and promotes their interaction for the formation of octamers, as has been suggested by Frousios et al. [28]. At the same time, our results indeed support the idea that protein–protein interaction surfaces and ‘aggregation-prone’ segments overlap in the homooligomeric form of proteins [46], since LQVVR is both a peptide with high aggregation propensity and a crystal contact [48].

In analogy to the model proposed by Staniforth et al. [49], based on the amyloidogenic properties of the peptide LQVVR and on the packing observed in the crystal structure 1R4C [17], we propose the model shown in Supplementary Fig. S3 as a plausible model of the amyloid fibrils formed by HCC. These fibrils have a diameter ca. 90–100 Å.

In this respect, it is interesting to note that, recent studies created a stabilized monomer of HCC using an engineered disulfide bond (L47C)–(G69C) between the structural elements that become separated upon domain swapping. Apart from the two well-conserved disulfide bridges of HCC which support the folding of the monomer, crystallographers created a brand new monomer-stabilizing disulfide bridge. They found that it is possible to inhibit dimerization, further oligomerization and finally amyloid formation of HCC by site-directed mutagenesis of its sequence. One of the mutant amino acids was Leu47 which is part of  $^{47}\text{LQVVR}^{51}$  [5].

For Icelandic Cerebral Angiopathy treatment, remedies/drugs designed to prevent aggregation of the LQVVR peptide, may prove to be of paramount importance in future work, following the example of recent impressive studies on transthyretin amyloidosis [50].

## Notes

The authors declare no competing financial interests.

## Acknowledgments

We thank the University of Athens for support. We should also like to thank EMBL, Heidelberg for hospitality and Mr. Peter Everitt for excellent technical assistance. We would also like to thank the editor of this manuscript for properly handling it and the anonymous reviewers for their useful and constructive criticism.

## Appendix A. Supplementary data

Supplementary data associated with this article can be found, in the online version, at <http://dx.doi.org/10.1016/j.febslet.2014.11.041>.

## References

- Abrahamson, M., Alvarez-Fernandez, M. and Nathanson, C.M. (2003) Cystatins. *Biochem. Soc. Symp.*, 179–199.
- Grubb, A. and Lofberg, H. (1982) Human gamma-trace, a basic microprotein: amino acid sequence and presence in the adenohypophysis. *Proc. Natl. Acad. Sci. U.S.A.* 79, 3024–3027.
- Grubb, A.O. (2000) Cystatin C-properties and use as diagnostic marker. *Adv. Clin. Chem.* 35, 63–99.
- Abrahamson, M., Barrett, A.J., Salvesen, G. and Grubb, A. (1986) Isolation of six cysteine proteinase inhibitors from human urine. Their physicochemical and enzyme kinetic properties and concentrations in biological fluids. *J. Biol. Chem.* 261, 11282–11289.
- Kolodziejczyk, R., Michalska, K., Hernandez-Santoyo, A., Wahlbom, M., Grubb, A. and Jaskolski, M. (2010) Crystal structure of human cystatin C stabilized against amyloid formation. *FEBS J.* 277, 1726–1737.
- Abrahamson, M., Grubb, A., Olafsson, I. and Lundwall, A. (1987) Molecular cloning and sequence analysis of cDNA coding for the precursor of the human cysteine proteinase inhibitor cystatin C. *FEBS Lett.* 216, 229–233.
- Bode, W. et al. (1988) The 2.0 Å X-ray crystal structure of chicken egg white cystatin and its possible mode of interaction with cysteine proteinases. *EMBO J.* 7, 2593–2599.
- Zerovnik, E. (2009) The emerging role of cystatins in Alzheimer's disease. *BioEssays* 31, 597–599.
- Johansson, L., Grubb, A., Abrahamson, M., Kasprzykowski, F., Kasprzykowska, R., Grzonka, Z. and Lerner, U.H. (2000) A peptidyl derivative structurally based on the inhibitory center of cystatin C inhibits bone resorption in vitro. *Bone* 26, 451–459.
- Revesz, T., Holton, J.L., Lashley, T., Plant, G., Frangione, B., Rostagno, A. and Ghiso, J. (2009) Genetics and molecular pathogenesis of sporadic and hereditary cerebral amyloid angiopathies. *Acta Neuropathol.* 118, 115–130.
- Ghiso, J., Pons-Estel, B. and Frangione, B. (1986) Hereditary cerebral amyloid angiopathy: the amyloid fibrils contain a protein which is a variant of cystatin

- C, an inhibitor of lysosomal cysteine proteases. *Biochem. Biophys. Res. Commun.* 136, 548–554.
- [12] Ghiso, J., Jenson, O. and Frangione, B. (1986) Amyloid fibrils in hereditary cerebral hemorrhage with amyloidosis of Icelandic type is a variant of gamma-trace basic protein (cystatin C). *Proc. Natl. Acad. Sci. U.S.A.* 83, 2974–2978.
- [13] Yamada, M. (2000) Cerebral amyloid angiopathy: an overview. *Neuropathology* 20, 8–22.
- [14] Asgeirsson, B., Haebel, S., Thorsteinsson, L., Helgason, E., Gudmundsson, K.O., Gudmundsson, G. and Roepstorff, P. (1998) Hereditary cystatin C amyloid angiopathy: monitoring the presence of the Leu-68 → Gln cystatin C variant in cerebrospinal fluids and monocyte cultures by MS. *Biochem. J.* 329 (Pt 3), 497–503.
- [15] Olafsson, I. and Grubb, A. (2000) Hereditary cystatin C amyloid angiopathy. *Amyloid* 7, 70–79.
- [16] Rostagno, A., Holton, J.L., Lashley, T., Revesz, T. and Ghiso, J. (2010) Cerebral amyloidosis: amyloid subunits, mutants and phenotypes. *Cell. Mol. Life Sci.* 67, 581–600.
- [17] Janowski, R., Abrahamson, M., Grubb, A. and Jaskolski, M. (2004) Domain swapping in N-truncated human cystatin C. *J. Mol. Biol.* 341, 151–160.
- [18] Liu, Y. and Eisenberg, D. (2002) 3D domain swapping: as domains continue to swap. *Protein Sci.* 11, 1285–1299.
- [19] Nelson, R. and Eisenberg, D. (2006) Recent atomic models of amyloid fibril structure. *Curr. Opin. Struct. Biol.* 16, 260–265.
- [20] Nelson, R. and Eisenberg, D. (2006) Structural models of amyloid-like fibrils. *Adv. Protein Chem.* 73, 235–282.
- [21] Kelly, J.W. (1996) Alternative conformations of amyloidogenic proteins govern their behavior. *Curr. Opin. Struct. Biol.* 6, 11–17.
- [22] Zerovnik, E. (2002) Amyloid-fibril formation. Proposed mechanisms and relevance to conformational disease. *Eur. J. Biochem.* 269, 3362–3371.
- [23] Hamodrakas, S.J. (2011) Protein aggregation and amyloid fibril formation prediction software from primary sequence: towards controlling the formation of bacterial inclusion bodies. *FEBS J.* 278, 2428–2435.
- [24] Sunde, M. and Blake, C.C. (1998) From the globular to the fibrous state: protein structure and structural conversion in amyloid formation. *Q. Rev. Biophys.* 31, 1–39.
- [25] Lopez de la Paz, M. and Serrano, L. (2004) Sequence determinants of amyloid fibril formation. *Proc. Natl. Acad. Sci. U.S.A.* 101, 87–92.
- [26] Esteras-Chopo, A., Serrano, L. and Lopez de la Paz, M. (2005) The amyloid stretch hypothesis: recruiting proteins toward the dark side. *Proc. Natl. Acad. Sci. U.S.A.* 102, 16672–16677.
- [27] Teng, P.K. and Eisenberg, D. (2009) Short protein segments can drive a non-fibrillizing protein into the amyloid state. *Protein Eng. Des. Sel.* 22, 531–536.
- [28] Frousios, K.K., Iconomidou, V.A., Karletidi, C.M. and Hamodrakas, S.J. (2009) Amyloidogenic determinants are usually not buried. *BMC Struct. Biol.* 9, 44.
- [29] Winn, M.D. et al. (2011) Overview of the CCP4 suite and current developments. *Acta Crystallogr. D Biol. Crystallogr.* 67, 235–242.
- [30] de Jongh, H.H., Goormaghtigh, E. and Ruyschaert, J.M. (1996) The different molar absorptivities of the secondary structure types in the amide I region: an attenuated total reflection infrared study on globular proteins. *Anal. Biochem.* 242, 95–103.
- [31] Savitsky, A. and Golay, M.J.E. (1964) Smoothing and differentiation of data by simplified least-squares procedures. *Anal. Chem.* 36, 1627–1639.
- [32] Blundell, T.L. and Johnson, L.N. (1976) *Protein Crystallography*, Academic Press, London-New York-San Francisco.
- [33] Berman, H.M., Westbrook, J., Feng, Z., Gilliland, G., Bhat, T.N., Weissig, H., Shindyalov, I.N. and Bourne, P.E. (2000) The protein data bank. *Nucleic Acids Res.* 28, 235–242.
- [34] Delano, W.L. (2005) *The PyMOL Molecular Graphics System*, DeLano Scientific LLC.
- [35] Surewicz, W.K., Mantsch, H.H. and Chapman, D. (1993) Determination of protein secondary structure by Fourier transform infrared spectroscopy: a critical assessment. *Biochemistry* 32, 389–394.
- [36] Jackson, M. and Mantsch, H.H. (1995) The use and misuse of FTIR spectroscopy in the determination of protein structure. *Crit. Rev. Biochem. Mol. Biol.* 30, 95–120.
- [37] Haris, P.I. and Chapman, D. (1995) The conformational analysis of peptides using Fourier transform IR spectroscopy. *Biopolymers* 37, 251–263.
- [38] Krimm, S. and Bandekar, J. (1986) Vibrational spectroscopy and conformation of peptides, polypeptides, and proteins. *Adv. Protein Chem.* 38, 181–364.
- [39] Valenti, L.E., Paci, M.B., De Pauli, C.P. and Giacomelli, C.E. (2011) Infrared study of trifluoroacetic acid unpurified synthetic peptides in aqueous solution: trifluoroacetic acid removal and band assignment. *Anal. Biochem.* 410, 118–123.
- [40] Rochet, J.C. and Lansbury Jr., P.T. (2000) Amyloid fibrillogenesis: themes and variations. *Curr. Opin. Struct. Biol.* 10, 60–68.
- [41] Chiti, F., Webster, P., Taddei, N., Clark, A., Stefani, M., Ramponi, G. and Dobson, C.M. (1999) Designing conditions for in vitro formation of amyloid protofibrils and fibrils. *Proc. Natl. Acad. Sci. U.S.A.* 96, 3590–3594.
- [42] Kelly, J.W. (2000) Mechanisms of amyloidogenesis. *Nat. Struct. Biol.* 7, 824–826.
- [43] Chiti, F. and Dobson, C.M. (2009) Amyloid formation by globular proteins under native conditions. *Nat. Chem. Biol.* 5, 15–22.
- [44] Hamodrakas, S.J., Hoenger, A. and Iconomidou, V.A. (2004) Amyloid fibrillogenesis of silkworm chorion protein peptide-analogues via a liquid-crystalline intermediate phase. *J. Struct. Biol.* 145, 226–235.
- [45] Shtukenberg, A.G., Punin, Y.O., Gunn, E. and Kahr, B. (2012) Spherulites. *Chem. Rev.* 112, 1805–1838.
- [46] Castillo, V. and Ventura, S. (2009) Amyloidogenic regions and interaction surfaces overlap in globular proteins related to conformational diseases. *PLoS Comput. Biol.* 5, e1000476.
- [47] Wahlbom, M., Wang, X., Lindstrom, V., Carlemalm, E., Jaskolski, M. and Grubb, A. (2007) Fibrillogenic oligomers of human cystatin C are formed by propagated domain swapping. *J. Biol. Chem.* 282, 18318–18326.
- [48] Janin, J. (1997) Specific versus non-specific contacts in protein crystals. *Nat. Struct. Biol.* 4, 973–974.
- [49] Staniforth, R.A., Giannini, S., Higgins, L.D., Conroy, M.J., Hounslow, A.M., Jerala, R., Craven, C.J. and Waltho, J.P. (2001) Three-dimensional domain swapping in the folded and molten-globule states of cystatins, an amyloid-forming structural superfamily. *EMBO J.* 20, 4774–4781.
- [50] Connelly, S., Choi, S., Johnson, S.M., Kelly, J.W. and Wilson, I.A. (2010) Structure-based design of kinetic stabilizers that ameliorate the transthyretin amyloidosis. *Curr. Opin. Struct. Biol.* 20, 54–62.